eJNDT e-Journal of Nondestructive Testing - ISSN 1435-4934 - www.ndt.net

EWSHM 2024
11th European Workshop on Structural Health Monitoring

Effect of Cryogenic Temperatures on Guided Waves Structural Health Monitoring Using Acousto-Ultrasonic Piezocomposite Transducers on Composite Structures

S. GALIANA [1,2*], M. MOIX-BONET [1,2], D. SCHMIDT [1], P. WIERACH [1,2]
[1] Deutsches Zentrum für Luft- und Raumfahrt, Braunschweig, Germany
[2] TU Clausthal, Clausthal-Zellerfeld, Germany
*email: shankar.galiana@dlr.de

Abstract. Composite materials have proven to be one of the ideal choices when it comes to structural applications requiring high performance working at extreme low temperatures, such as hydrogen tanks or space structures. One of the main challenges of using them is that they are susceptible to impact and fatigue, which may lead to different damages. Implementing structural health monitoring (SHM) systems is one strategy to enhancing their reliability, with guided waves (GW) being one of the most promising techniques. For the effective implementation of GW-based SHM in these applications, an in-depth comprehension of its behavior up to cryogenic temperatures is required for accurate monitoring. In this regard, the objective of the present work is to preliminary investigate the effect of low temperatures on wave propagation and transducer integration. By progressively removing a composite panel from a liquid nitrogen (LN_2) bath with an integrated GW-SHM network based on co-bonded DuraAct™ transducers, the GW and temperature are continuously monitored from LN_2 CT to room temperature. The results show that the behavior of the GW by decreasing the temperature does not follow a monotonic pattern, having at least local maxima in terms of amplitude, and nonlinear behavior for the time-of-flight. Electromechanical impedance and C-Scans ensured the quality of the bonding of the co-bonded DuraAct™ transducers.

Keywords: Structural Health Monitoring, Cryogenic temperatures, DuraAct™, Guided waves

Media and Publishing
https://doi.org/10.58286/29667

Introduction

Composite materials have not stopped growing in the past few years for their unique properties, such as high specific strength, especially in applications like hydrogen tanks or space structures that are required to be operated at extreme low temperatures [1]. Despite the fact that composite materials, and in particular carbon-fiber reinforced polymers (CFRP), are proven to be one of the best choices for these applications [2], they are susceptible to impact and fatigue damages, such as microcracks, cracks, and delaminations, decreasing their desirable properties and the reliability of the structure [3]. With this in mind, one possible strategy for enhancing composite structure reliability is to continuously monitor them using structural health monitoring (SHM) systems, where guided waves (GW) are a promising technique [4].

One of the main advantages of GW is their sensitivity to small damages such as cracks or delaminations [5], but at the same time, they are very sensitive to any state of the monitored structure, such as mechanical loads or environmental conditions, especially moisture and temperature [6, 7]. Since GW-SHM relies on changes between the GW signals of a pristine state of the structure and the GW signals of the desired monitored state, any deviation in the system conditions has a big impact that can mask a possible damage or give false positive.

The elastic and viscoelastic properties of CFRP vary with temperature, as do the laminate's internal residual stresses. Composites become stiffer at lower temperatures, particularly in the transverse direction relative to the fiber direction, with less affection in the longitudinal direction due to the greater influence of the polymeric matrix on transverse properties [8]. These properties are strongly connected to how GW propagates, and any changes have a direct impact on them. In addition, large temperature variations affect not only the structure's properties and wave propagation throughout it, but also the behavior of the transducer and how waves are transmitted and received. Transducer materials used for sending and receiving acousto-ultrasonic signals are typically soft lead titanate zirconate (PZT) piezoceramics, whose functionality degrades significantly with temperature decrease far from Curie temperature [9]. For this reason, in order to effectively implement the GW-SHM in applications requiring function in low-temperature environments, an on-depth understanding of the system behavior up to cryogenic temperatures (CT) is needed for accurate monitoring.

In this regard, the objective of the present work is to preliminary investigate the effect of low temperatures on co-bonded DuraAct^{TM} acousto-ultrasonic piezocomposite transducers, their bonding to the structure, and wave propagation. The measurements are taken on a CFRP panel laminate with an integrated co-bonded DuraAct^{TM} transducer network.

The effect of low temperatures on bonding and piezoelectric properties of the transducers is evaluated by measuring the electromechanical impedance (EMI) at room temperature (RT) and at liquid nitrogen (LN_2) CT for different transducer configurations. The bonding assessment is additionally verified with an exhaustive C-scan of the panel.

The effect of low temperatures on the GW is addressed by gradually removing the composite panel from an LN_2 bath while constantly recording the GWs and temperature at various frequencies. The recorded GW signals are then evaluated and compared to measured temperatures ranging from LN_2 CT to RT, as well as frequencies of 50, 70, 100, and 150kHz.

1. Materials and Methods

1.1. Specimen configuration

The study uses co-bonded DuraAct™ transducers onto CFRP panel for the evaluation of the GW-SHM system under cryogenic temperatures. DuraAct™ is a commercially available acousto-ultrasonic thermoset piezocomposite transducer consisting of a soft PZT (PIC255 from PI-Ceramic GmbH) covered on both sides by an electrode contacted with a metallized polyester fleece. The transducer is embedded in an external electrically insulating ductile polyester fleece-reinforced polymer laminate, and it includes two contact points for soldering the wires [10].

In order to differentiate the effect of LN_2 CT over the different parts of the system, three different transducer scale configurations are used. First, a free piezoceramic disc of 10mm diameter and 0.2mm thickness used on DuraAct™ transducers' manufacturing depicted in **Fig. 1 (a)**, is used to evaluate the effect of LN_2 CT on the piezoceramic EMI. Second, an unintegrated DuraAct™ transducer depicted in **Fig. 1 (b)** is used to evaluate the effects of LN_2 CT on EMI coming from the embedment composite. Finally, a set of DuraAct™ transducers are co-bonded onto a CFRP panel as depicted in **Fig. 1 (c)**, and tested for the GW-SHM temperature behaviour evaluation and EMI response under LN_2 CT.

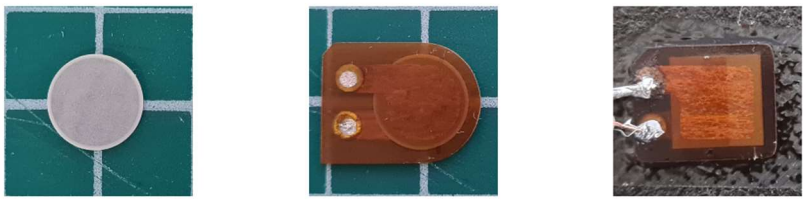

(a) (b) (c)

Fig. 1. (a) Piezoceramic, (b) DuraAct™ transducer and (c) Co-bonded DuraAct™ transducer.

The CFRP panel used for the GW-SHM temperature behaviour evaluation is made by automated tape placement with Hexply AS4/8552 with a nominal thickness of 0.18mm and $[45/0/-45/90/0/90]_S$ stacking sequence laminate of 550mm×550mm. Once the prepreg laminate is made, DuraAct™ transducers are place strategically distributed onto the panel in two rows, separated by 300mm, with four transducers in each row, and a 100 mm separation between them as depicted in **Fig. 2 (a)**. The entire laminate with the transducers is then cured in an autoclave process resulting in a 2.2mm panel thickness. Finally, the edges of the 550mm×550mm panel are trimmed to eliminate manufacturing defects, resulting in a final dimension of 500mm×450mm.

Mechanical properties of Hexply AS4/8552 used for analytical approximations are resumed in **Table 1**. RT values are taken directly from literature [11], while LN_2 CT properties, are estimated by applying different coefficients to RT properties according to literature [12]. Values for -65ºc are lineally approximated from RT and LN_2 CT data.

Table 1. Estimated Hexply AS4/8552 mechanical properties for RT, LN_2 CT and -65ºC.

	RT	LN_2 CT	L(x) -65ºC		RT	LN_2 CT	L(x) -65ºC		RT	LN_2 CT	L(x) -65ºC
E_1 (GPa)	141	135.1	138.7	G_{12} (GPa)	5.3	7.5	6.2	ν_{12}	0.32	0.23	0.29
E_2 (GPa)	9.6	12.8	10.9	G_{13} (GPa)	5.3	7.5	6.2	ν_{13}	0.32	0.23	0.29
E_3 (GPa)	9.6	12.8	10.9	G_{23} (GPa)	3.4	6.1	4.5	ν_{23}	0.49	0.47	0.48

1.2. Thermal test set-up

The study is divided in two parts. The first part aims to investigate the effect of LN_2 CT on piezocomposite transducer bonding and electromechanical response. Meanwhile, the second part, is intended to assess the behaviour of the GW-SHM at various temperatures, ranging from LN_2 CT to RT. Experimental test setup is shown in **Fig. 2 (c)**, together with the temperature on which the data points are collected (**Fig. 2 (b)**).

For the first part of the study, the three different transducer scale systems configurations are connected to a Cypher Instruments Ltd. C-60 impedance analyzer and measured before, during, and after complete immersion in a LN_2 bath. In case of the co-bonded configuration, the process is repeated several times to evaluate if there is any change over the process cycles. Also, the CFRP panel with the integrated co-bonded transducer network is analyzed by C-Scan in the pristine state and after thermal cycling process.

For the second part, the transducer network is connected with coaxial cables to a GW-SHM data acquisition platform based on the PXIe technology of National Instruments Corp. with a thermocouple in the CFRP panel surface. The panel is immersed in an LN_2 bath until it reaches LN_2 CT (-197ºC). After is gradually removed from the bath and heated from LN_2 CT until reaching RT (20ºC) while continuously recording the GW at 50, 70, 100 and 150kHz together with the temperature. Additionally, an extended GW frequency range of 40kHz to 300kHz in steps of 10 kHz is recorded for LN_2 CT and RT.

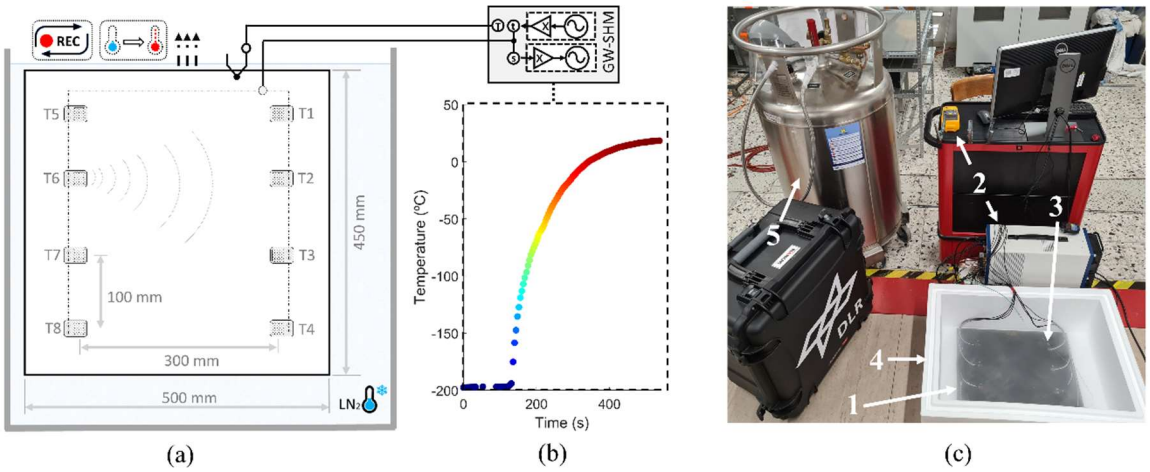

Fig. 2. (a) Schematic representation of test set-up with (b) temperature datapoints over time and (c) test set-up where (1) CFRP panel specimen, (2) data acquisition systems, (3) thermocouple, (4) LN_2 bath and (5) LN_2 tank.

2. Results and Discussions

2.1. Transducer electromechanical and bonding thermal effect

EMI measurements of a pristine state at RT, at LN_2 CT, and RT after cooling are presented for a free PZT disc in **Fig. 3 (a)**, a free DuraAct^{TM} in **Fig. 3 (b)**, and a co-bonded DuraAct^{TM} in **Fig. 3 (c)**. Measurements on free PZT and co-bonded DuraAct^{TM} show negligible permanent effects between before and after thermal exposure. In contrast, the free DuraAct^{TM} transducer exhibits minor remnant changes. This phenomenon could be attributed to the shift in the DuraAct^{TM} transducers' characteristic residual compression stress state following thermal loading. It is interesting that this effect is not observed in the co-bonded scenario; this could be due to the coupled electro-mechanical system, which constricts the entire piezocomposite transducer to the CFRP plate.

Impedance values at LN_2 CT are higher in all cases compared to RT with a resonance and antiresonance frequency shifted towards higher frequencies. This effect is due to the loss of piezoelectric properties when highly decreasing temperature and might have an impact when using it as a transducer.

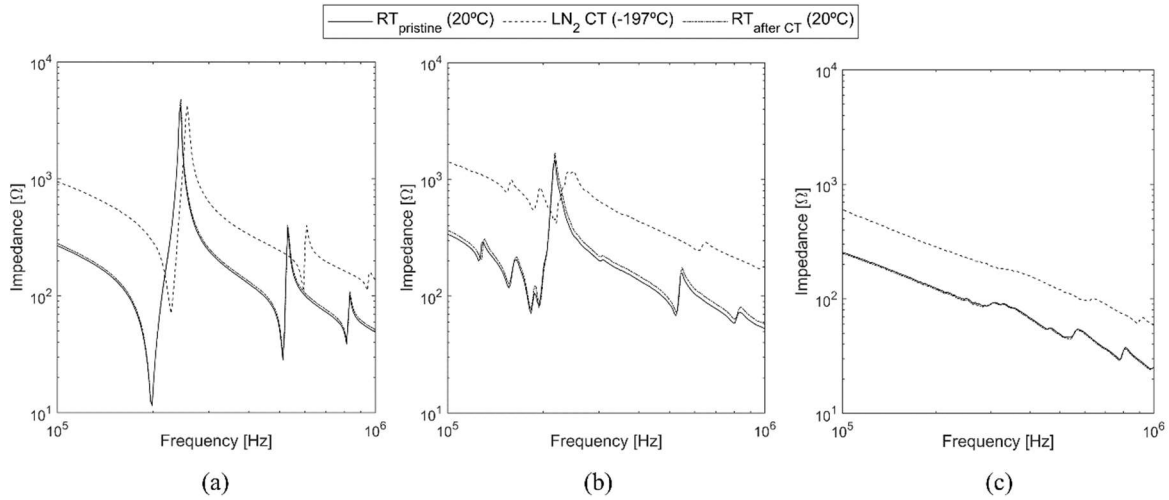

Fig. 3. EMI for (a) free piezoceramic ø10mm disc, (b) free DuraAct™ and (c) co-bonded DuraAct™ at RT previous to cryogenic temperature, at LN_2 CT and at RT posterior to cryogenic temperature.

No significant changes are noticed in co-bonded transducers after cycling from RT to LN_2 CT in the EMI or the C-Scan. **Fig. 4 (a)** depicts the EMI response at RT following each temperature cycle from RT to LN_2 CT and back to RT. The small variations do not follow a monotonic pattern with temperature, being in some cases higher and in some cases lower than the pristine state. These minor variances could be due to variations in room temperature or measurement clamping. **Fig. 4 (b)** and **(c)** depicts the normalized C-Scan of the selected co-bonded transducers used for data analysis before and after the LN_2 cryo-cycling, respectively. Furthermore, in **Fig. 4 (d),** the normalized signal from both C-Scans is subtracted and plotted to identify potential variations following the thermal cycle. Only slight signal changes can be noticed at the transducer's edges and in the electrical contacts. The edge differences could be attributed to the misalignment of the two C-Scan methods. Differences in electric contacts could be attributed to soldering and desoldering of the signal wires between the two C-Scans.

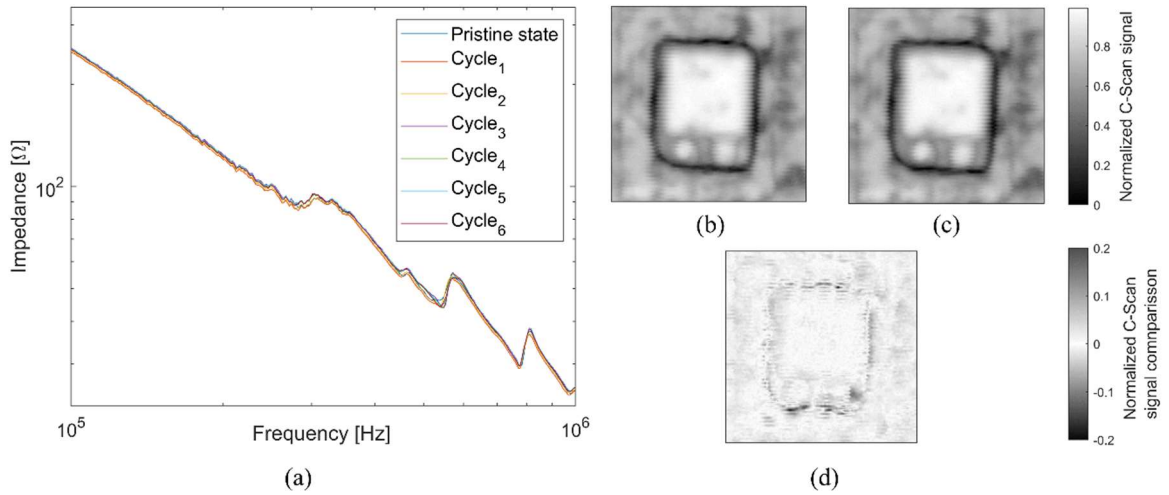

Fig. 4. (a) Thermal cryogenic cycling co-bonded DuraAct™ EMI and C-Scans for (b) pristine co-bonded DuraAct™, (c) thermal cryogenic cycled co-bonded DuraAct™, and (d) C-Scan signal subtraction.

2.2. GW-SHM thermal effect

The GW-SHM temperature effect is evaluated using an actuation signal consisting of a 5-pulse sine wave with a Hanning window and an amplitude of 5 volts amplified by a factor of 10 at frequencies of 50, 70, 100, and 150kHz. The sensing signal is further processed by denoising and determining the envelope and envelope peaks for each mode. Envelope signal measurements for the various frequencies from transducer 3 and sensor 7 used for the analysis are shown for 50, 70, 100, and 150kHz in **Fig. 5**.

Because of the low amplitude and overlapping reflections at higher frequencies, the maximum amplitude of A_0 mode is only determined between 50 and 70 kHz, whereas S_0 mode is determined for the entire frequency range. For A_0 mode, the envelope signal at 50 and 70 kHz at LN_2 CT has a mainly zero amplitude. This effect results from the fact that the envelopes were taken while the panel was submerged in LN_2. Out-of-plane component of A_0 mode, are strongly influenced by radiation in adjacent media and exhibit high attenuation in liquid media compared to air. This effect is minimal in the case of S_0 mode at any of the tested frequencies.

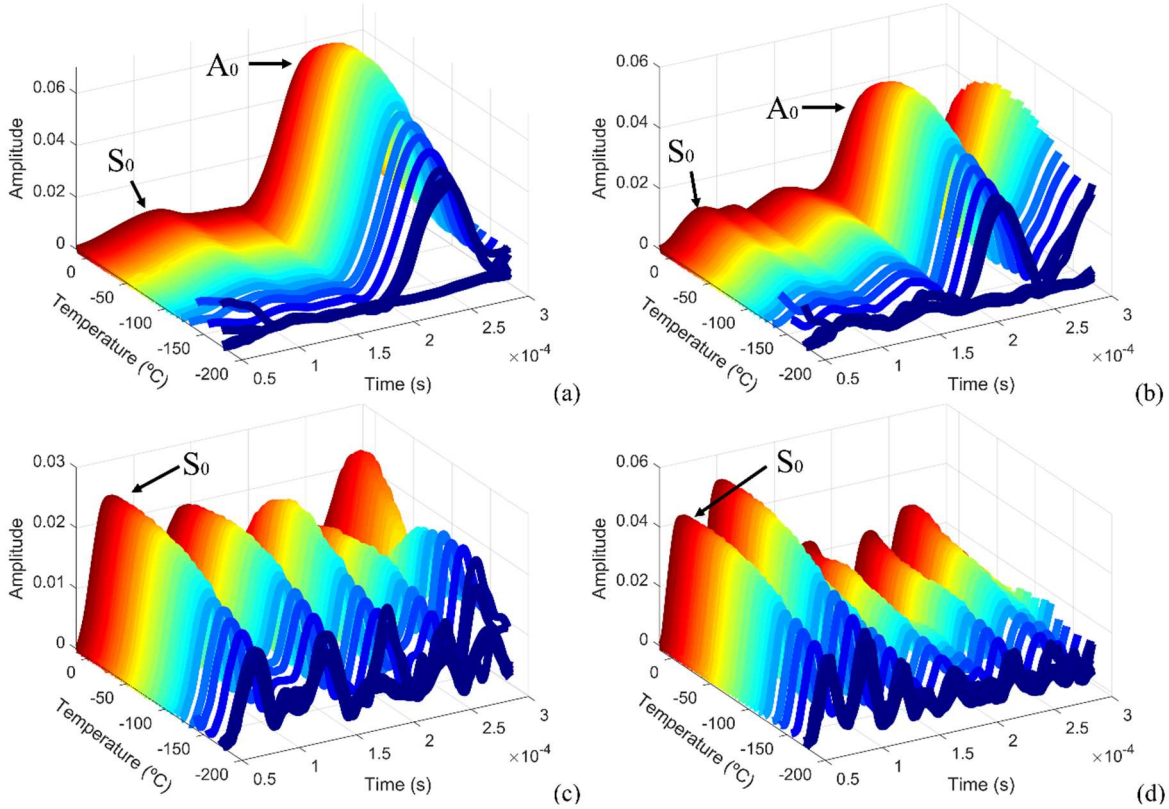

Fig. 5. Signal envelope for temperatures varying from RT to LN_2 CT for (a) 50kHz, (b) 70kHz, (c) 100kHz and (d) 150kHz.

To assess the temperature effect across modes, maximum amplitude and its time of flight (ToF), excluding the data collected when the panel was submerged in the LN_2 bath, are analyzed against temperature ranges for S_0 and A_0 modes for the different frequencies.

When analyzing the amplitudes from the envelope peaks corresponding to the S_0 and A_0 modes depicted in **Fig. 6**, on the S_0 mode, amplitudes are higher at higher frequencies. In contrast, for A_0 mode, the amplitude at 50 kHz is higher than 70 kHz. S_0 mode amplitudes slightly increases when decreasing temperature, reaching a maximum at around -65ºC for 50 and 70 kHz, and around -15ºC for 100 and 150 kHz. After gradually decreases at a higher ratio for higher frequencies. A_0 mode amplitudes in both frequencies notoriously increase

when decreasing temperature until reaching a maximum at around -65ºC, and then decrease with a higher ratio at lower frequencies.

In both modes, the change of amplitude relative to temperature over -65ºC has an exponential behavior, while below this temperature, the amplitude change behaves more linearly. Furthermore, the behavior of the amplitude over frequency is consistent for all frequencies in each mode without any significant shift over temperature, with the difference between frequencies being greater near the maximum peak and decreasing as it moves away.

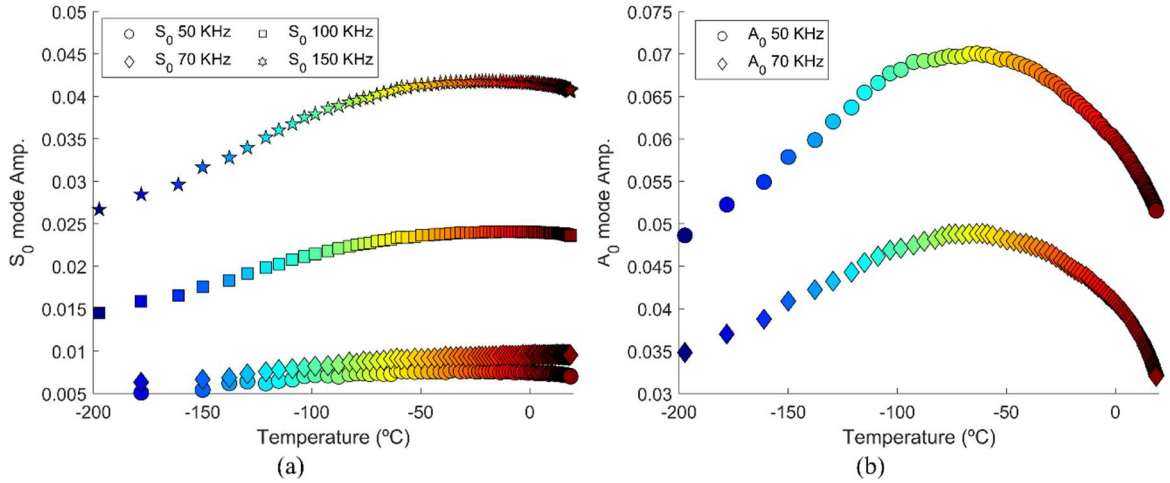

Fig. 6. Amplitude of (a) S_0 mode and (b) A_0 mode over temperature range for 50, 70, 100 and 150kHz.

When analyzing the ToF from the envelope peaks corresponding to the S_0 and A_0 modes depicted in **Fig. 7**, on the S_0 mode, it does not change significantly over the temperature range for any frequency range, behaving mainly linearly. Some higher dispersion appears below -100 ºC for all frequencies, especially on 50kHz, where some of the datapoints are omitted in the plot because they were out of range, mainly because of envelope signal processing and equipment limitations with cross-talk. The values do not follow a monotonic behavior with the frequency, where the maximum ToFs are at 50kHz at around 60µs, the lower are at 70Khz at around 45µs, and in between for 100 and 150kHz at around 50µs. On the A_0 mode, values for 50kHz are higher than 70kHz. In both frequencies, the ToF decreases considerably with the decrease in temperature, with a higher ratios and exponential behavior at temperatures closer to RT and at lower ratios and more linear behavior below -65ºC.

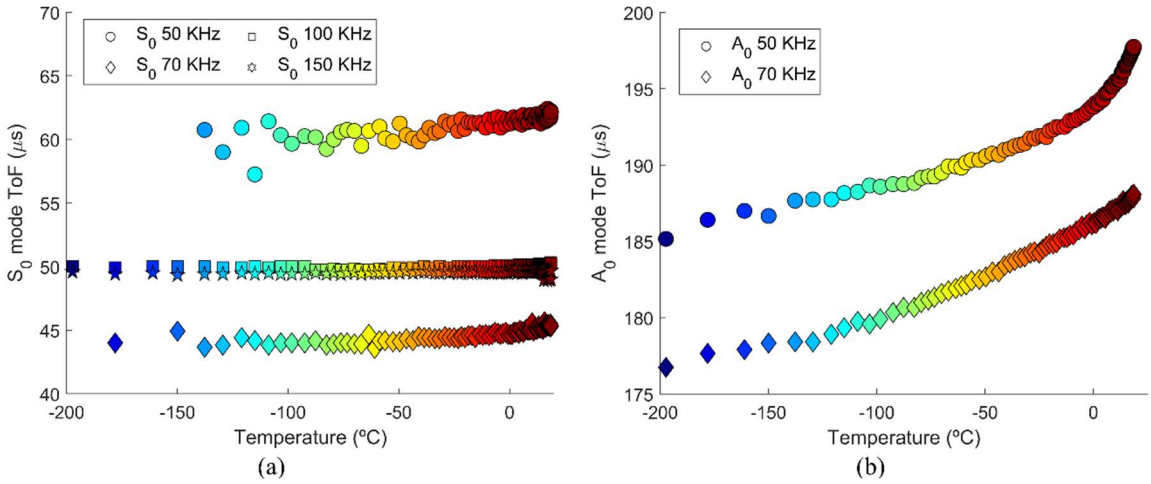

Fig. 7. ToF of (a) S_0 mode and (b) A_0 mode over temperature range for 50, 70, 100 and 150kHz.

To better understand how temperature drives signal changes, a first analytical approximation of the ToF spectrum dispersion curves shown in **Fig. 8 (a)** and an amplitude spectrum dispersion curve estimation using the Sinc fitting equation shown in **Fig. 8 (b)** are analyzed for RT, LN_2 CT, and -65ºC, which is the temperature with the maximum amplitude peak. Data points for RT are obtained from the extended frequency GW-SHM in both modes to better represent the behavior across the frequency range, as well as for LN_2 CT in S_0 mode. Data for LN_2 CT A_0 mode and -65ºC modes are based on previously examined data.

An analytical approximation for ToF made using the mechanical properties defined in **Table 1** within the Dispersion Calculator[2] Version from the German Aerospace Center [13] shows minimal change for S_0 mode for the various temperatures, which is consistent with the data points for all analyzed temperatures. Furthermore, for A_0 mode at RT, the analytical model fits the experimental data with a slight shift toward lower frequencies. For A_0 mode at LN_2 CT and -65ºC, the analytical model underestimates the ToF, but captures the overall effect of lowering ToF. The difference could be due to a lack of accurate material properties to define the real and imaginary parts of the stiffness matrix for the defined temperatures, but it is reasonable to assume that changes in stiffness matrix parameters drive ToF temperature behavior by changing phase velocities.

According to Sinc fitted amplitude dispersion curves, the maximum amplitude for the A_0 mode at RT is approximately 40 kHz. Shifting the maximum amplitude to higher frequencies, amplitudes at 50 and 70 kHz will never approach the magnitudes of -65ºC. This impact eliminates the hypothesis that the increase in amplitude could be caused by a shift in maximum amplitude to higher frequencies. For S_0 mode, Sinc fitting curves reveal moderate changes between RT and -65ºC and has significant change when compared to LN_2.

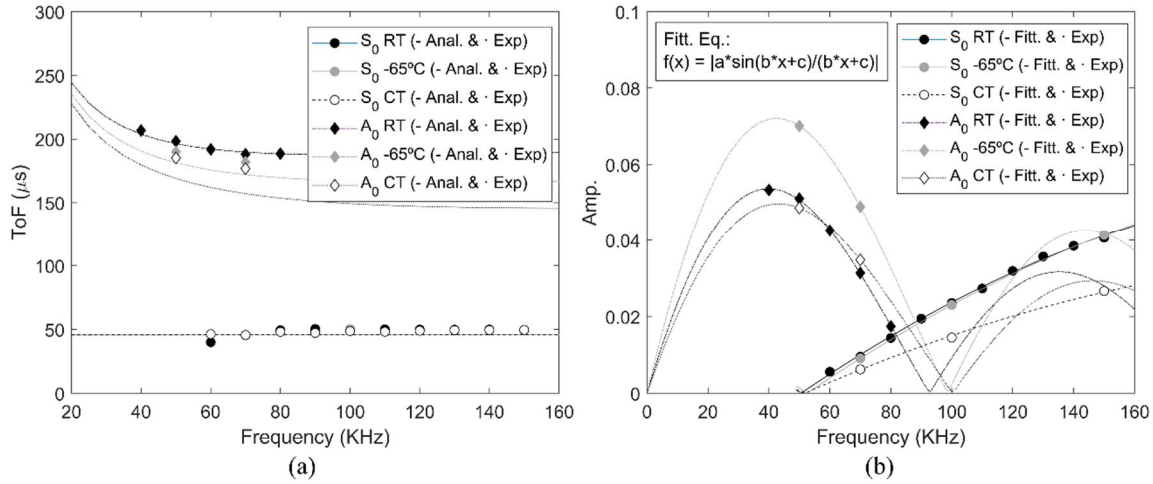

Fig. 8. (a) Analytical ToF dispersion curve with respect to measurement data and (b) fitted amplitude dispersion curve with respect to measurement data.

Assuming that the bonding does not change, as indicated by the EMI and C-scan, and that the change in properties of the interface between piezoceramic and the CFRP panel is negligible for co-bonded transducers, the effects on amplitude and ToF change must be attributed to CFRP and piezoceramic properties.

According to the authors, the shift in amplitude might be explained by the fact that when the temperature drops, the stiffness and viscoelastic properties of the CFRP improve, resulting in lower signal attenuation and, as a result, higher amplitude. At the same time, as temperature decreases, so do piezoelectric properties, resulting in decreased amplitudes. The amplitude behavior can be explained as follows: from RT to -65ºC, the CFRP properties change dominates and causes amplitudes to rise, whereas below -65ºC, the loss of

piezoceramic characteristics leads to amplitude reduction as schematically represented in **Fig. 9**.

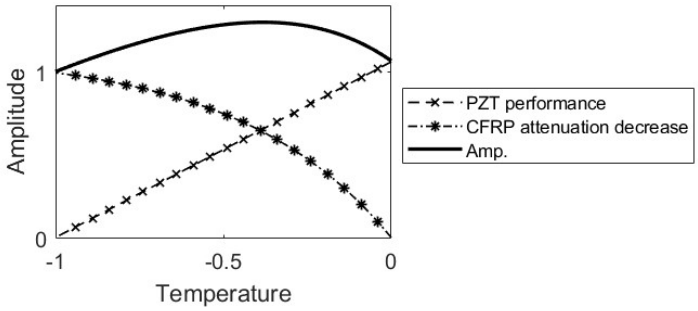

Fig. 9. Schematically representation of amplitude performance driven parameters.

3. Conclusions

The study's findings reveal that the bonding and transducer health is insignificantly affected by thermal cycling loads, proving the effectiveness of the chosen integration method and transducer. At the same time, it demonstrates the complex behavior of GW when monitoring composite structures at temperatures ranging from RT to CT.

The research on GW-SHM temperature effects revealed that amplitudes do not follow a monotonic pattern when the temperature is reduced, with at least local maxima in terms of amplitude and nonlinear behavior for ToF, leading future work to determine appropriate temperature compensation factors. Furthermore, the significant differences in the amplitude of the A_0 mode recorded between air and liquid media add a new dimension to the complexity of operating GW-SHM in real CT environments. In fact, low temperatures can condensate atmospheric gases into the monitored structure or form ice on the surface, completely altering wave propagation.

As a preliminary investigation, it was not possible to properly identify the parameter changes over temperature of the piezoceramics and CFRP, but the study discovered that these are critical to an in-depth understanding of the temperature-driven effects. Despite the study's plausible explanation for the amplitude and ToF behavior with temperature, more research is needed to validate and quantify these findings.

In conclusion, the preliminary study demonstrates the successful performance of the co-bonded DuraAct^{TM} as a reliable integration method and transducer solution for operating GW-SHM at extreme low temperatures, while also contributing to future work aimed at identifying temperature compensation factors that will allow for better and more reliable monitoring systems.

Funding

This project has received funding from the European Union's Horizon 2020 research and innovation programme under the Marie Sklodowska-Curie grant agreement No 859957 ''ENHAnCE, European training Network in intelligent prognostics and Health mAnagement in Composite structurEs''.

References

[1] Irving, S.P.E.; Soutis, C. Polymer Composites in the Aerospace Industry; Woodhead Publishing: Cambridge, UK, 2014.

[2] McCarville, D.A.; Guzman, J.C.; Dillon, A.K.; Jackson, J.R.; Birkland, J.O. 3.5 Design, Manufacture and Test of Cryotank Components; Elsevier: Amsterdam, The Netherlands, 2018; pp. 153–179.

[3] Talreja, R.; Singh, C.V. Damage and Failure of Composite Materials; Cambridge University Press: Cambridge, UK, 2012; Volume 605.

[4] Boller C., Chang F-K, Fujino Y., eds. Encyclopedia of Structural Health Monitoring. Chichester, UK: John Wiley & Sons, Ltd 2009.

[5] Janapati, V.; Kopsaftopoulos, F.; Li, F.L.; Lee, S.; Chang, F.-K. Damage Detection Sensitivity Characterization of Acousto-Ultrasound-based SHM Techniques. Struct. Health Monit. 2016, 15, 143–161.

[6] Eckstein B, Moix-Bonet M, Bach M (2014) Analysis of environmental and operational condition effects on guided ultrasonic waves in stiffened CFRP structures. EWSHM - 7th European Workshop on Structural Health Monitoring 2014, Nantes.

[7] Moix-Bonet M, Eckstein B, Wierach P (2018) Temperature compensation for damage detection in composite structures using guided waves. EWSHM - 9th European Workshop on Structural Health Monitoring 2018, Manchester.

[8] Sánchez-Sáez S, Gómez-del Río T, Barbero E, et al. Static behavior of CFRPs at low temperatures. Composites Part B 2002; 33: 383–390

[9] Zhang, X.L., Chen, Z., Cross, L.E., Schulze, W.A.: Dielectric and piezoelectric properties of modified lead titanate zirconate ceramics from 4.2 to 300 k. Journal of Materials Science 18, 968–972 (1983)

[10] Wierach P. Electromechanical functional module and associated process. US 6,930,439 B2, 528, 2005.

[11] Hexcel Corporation. HexPly ® 8552 Product Data Sheet. -EU Version pp. 1–6, 2016

[12] Sápi, Z.; Butler, R. Properties of cryogenic and low temperature composite materials—A review. Cryogenics 2020, 111, 103190.

[13] Huber, A. Dispersion Calculator 2.4 User's Manual; German Aerospace Center: Cologne, Germany, 2023.